Detection and Control of a Wheeled Mobile Robot Based on Magnetic Navigation

Guan Sun, Dan Feng, Youtong Zhang, Dongdong Weng
Beijing Institute of Technology
Beijing, China
xsunguanx@gmail.com

***Abstract*—This paper introduces the design of a wheeled mobile robot based on magnetic navigation. The working principle of magnetic navigation is analyzed, and a novel navigation path detection algorithm is proposed. Meanwhile, the fuzzy control algorithm and PID algorithm are combined to optimize the control performance of the steering servo and the electric motor. The experimental results show the effectiveness of both the detection and the control algorithm. The wheeled mobile robot can trace the navigation path automatically and precisely at a high speed.**

Keywords—Magnetic Navigation; Wheeled Mobile Robot; Path Detection Algorithm; Control Algorithm

I. INTRODUCTION

With the rapid developing of robotic technologies, wheeled mobile robots have been widely applied to various fields, especially those dangerous and harsh environments [1]. Automatic navigation technology is one of the key topics among all these robot researches. By utilizing different kinds of sensors, the navigation approaches of mobile robots can be classified into several categories such as magnetic field, inertia, vision and sonar. As a promising technology, magnetic navigation provides the advantages like high accuracy, perfect robustness, simple installation and low maintaining cost.

The study of magnetic navigation originated from 90s last century in United States and Japan. Recently, its applications in the field of intelligence transportation can be seen in many countries like United States, Netherlands and Japan [2]. Most present systems are based on permanent magnetic markers, which are discrete thus limits the accuracy and the speed of the navigation. On the other hand, few researches have been done on wire based magnetic navigation [3]. And there is also no mature solution to detect the navigation path precisely.

This paper introduces the system design of a wheeled mobile robot, in front of which the inductors are mounted as magnetic field sensors. Thus the robot can detect the magnetic field emitted by a navigation wire carrying altering current. The wire is embedded in the navigation path. A path-detecting algorithm is proposed to calculate the relative position between the robot and the navigation wire. Fuzzy control and PID algorithm are combined to control the direction and speed of the robot to achieve high-accuracy and high-speed automatic navigation. The effectiveness, robustness and applicability of this method have been verified through the experiments.

II. SYSTEM OVERVIEW

The wheeled mobile robot introduced in this paper is based on a four-wheel model car. The front wheels are driven by the servo through the steering connecting rods to control the direction of the robot, and the rear wheels are driven by the electric motor though transmission gears to control the speed of the robot. The magnetic sensors are distributed symmetrically in the front of the model car to increase the foresight, and the functional circuit boards and battery are mounted on the chassis of the model to lower down the center of gravity.

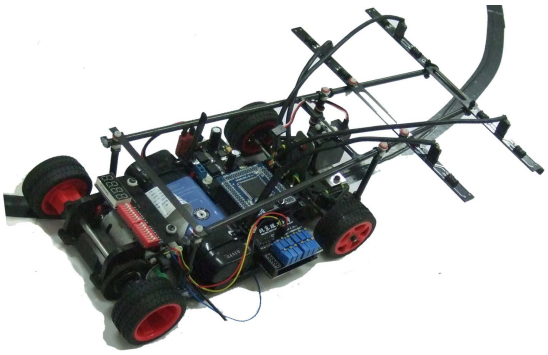

Fig. 1. The appearance of the wheeled mobile robot

The three dimensions of the wheeled mobile robot are $45\text{cm} \times 25\text{cm} \times 12\text{cm}$ (length × width × height), and the appearance of the robot is shown in Fig. 1, the overall system structure is shown in Fig.2.

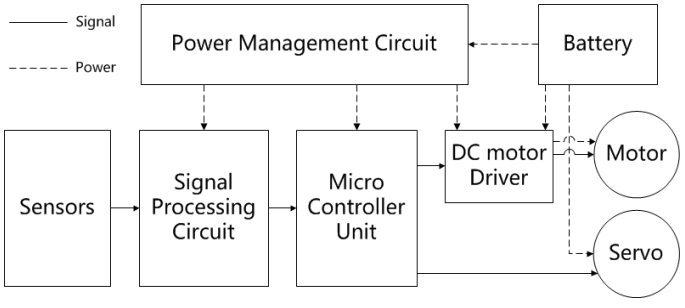

Fig. 2. The structure of the system

III. THE FUNDAMENTALS OF MAGNETIC NAVIGATION

A. Magnetic Field Source

As an essential medium to implement the navigation, a magnetic field source should be installed along the target path. By detecting the spatial distribution of magnetic field emitted by it, the wheeled mobile robot calculates its current position. In this system, an enameled wire carrying alternating current is built in the middle of the navigation path.

According to Maxwell's electromagnetic theory, the wire carrying alternating current will produce electric and magnetic field around it, of which the time and spatial distribution could be calculated. Hence the magnetic field could be utilized to calculate the distance between the source wire and the detecting sensors.

Due to the large scale difference between the robot and the source wire, the navigation wire can be regarded as infinite straight. Based on the Biot-Savart Law, the alternating magnetic field distribution can be derived as (1).

$$B = \frac{\mu_0 I}{2\pi r} sin\omega t \quad (1)$$

Where B is the magnetic field intensity,

μ_0 is the vacuum permeability,

I is the amplitude of the alternating current in the wire,

$Isin\omega t$ is the alternating current, and

R is the distance from a space point to the wire.

The distribution of the magnetic field around the navigation wire is like a series of concentric circles. The magnetic field intensity at each circle keeps constant but decreases as the radius (distance from the wire) increases.

B. Magnetic Field Sensors

Inductors are chosen as the magnetic field sensors, the coins of which are able to transfer the altering magnetic field intensity to voltage signal. The I-shape inductors in small size and with high quality factor are used in the system.

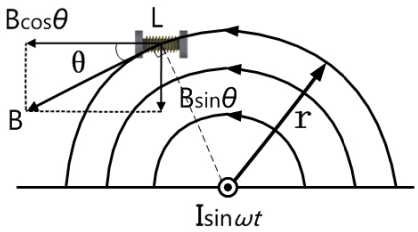

Fig. 3. A inductor sensor in the magnetic field emitted by the navigation wire

According to Faraday's law of electromagnetic induction, the voltage, as shown in Fig.3, sensed by the inductor is derived as (2).

$$E = -\frac{d\Phi(t)}{dt} = -NA\mu_r \frac{dB(t)}{dt} cos\theta = -\frac{NA\mu_0\mu_r}{2\pi}\frac{I}{r} cos\theta cos\omega t \quad (2)$$

Where E is the induced voltage,

Φ is the axial magnetic flux through the inductor,

N is the number of the coils of the inductor,

A is the transversal area of a coil,

μ_r is the permeability of the iron core of the inductor, and

θ is the angle between the axis of the inductor and the direction of magnetic field.

As (2), the induced voltage of a single inductor is a Cosine alternating signal. Its amplitude is directly proportional to the current intensity in the source wire, and the amplitude is inverse to the distance between the inductor and the source wire. It is also related to the angle between the central axis of the inductor and the direction of the magnetic field.

C. The Signal Processing Circuit

From the analysis above, the induced voltage which reflects the relative spatial position between the inductor and the navigation wire is alternating and not able to be calculated directly. In this system, the alternating signal is processed as an input, and the output is a direct current voltage signal which is proportional to the amplitude of the input signal.

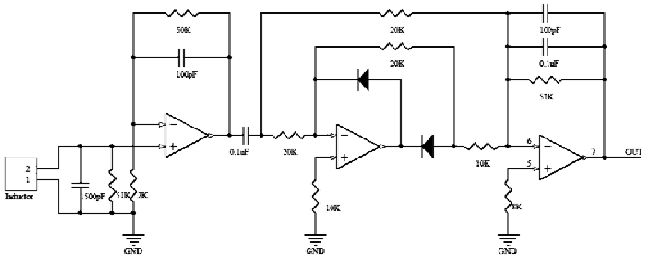

Fig. 4. The Schemstic Diagram of the Signal Processing Circuit

As the signal processing circuit is shown in Fig.4, the input signal goes through the LC resonant tank first. By matching the inductance and the capacitance value, the center frequency of the LC band-pass filter is equal to the frequency of the alternating magnetic field and the induced voltage. Thus the effective input signal is obtained and the interference signals are filtered out.

To measure the input signal precisely, the week signal after frequency-selecting is amplified from millivolt to volt level by the operational amplifier circuit.

The magnified signal is still alternating, then it is processed by a half bridge detection circuit consist of diodes and operational amplifiers to get the output direct current voltage. After analogue-to-digital conversion, the digitalized voltage value is utilized to calculate the navigation path.

IV. PATH DETECTION

A. Path calculation algorithm

Based on the distribution of magnetic field, the path calculation algorithm computes the relative spatial relationship between the sensors and the navigation wire to control the direction and the speed of the robot. The arrangement of the inductors derived from the algorithm directly results in the accuracy and the effectiveness of the path detection.

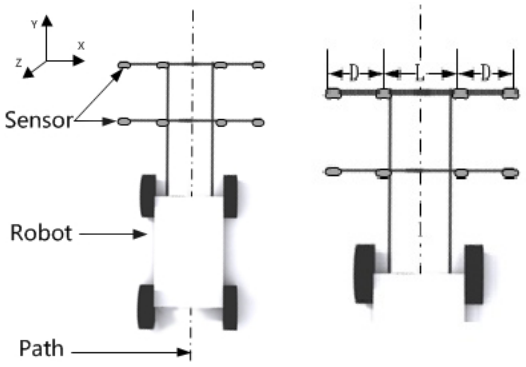

Fig. 5. The Distribution of the Sensors

Towards the control accuracy and the path prediction, eight inductors are separated in two rows and arranged horizontally in the front of the robot as shown in Fig. 5(a) and (b). D is the distance between two inductors in the same side. The interval between two inductors in the middle is L. All the sensors are at the same height *H*.

A right-handed coordinate system is built for the convenience of calculation and expression as Fig. 5(a), in which X axis is the horizontal direction perpendicular to the central axis of signal wire, Y axis is the heading direction and Z axis is the vertical direction perpendicular to the ground.

Taking the four inductors in the second row as an example, the coordinates of them are $L_1(x_1, 0, H)$ 、 $L_2(x_2, 0, H)$ 、 $L_3(x_3, 0, H)$ 、 $L_4(x_4, 0, H)$. For each sensor, its induced voltage can be derived as (3) according to (2).

$$E_i = K\frac{IH}{x_i^2+H^2}cos\omega t \ \ (i = 1,2,3,4) \tag{3}$$

Where the proportional constant can be deduced as (4).

$$K = -\frac{NA\mu_0\mu_r}{2\pi} \tag{4}$$

After the signal processing circuit, the altering signals are transferred by AD conversion. The magnitude of the direct voltage was shown as (5).

$$U_i = KK'\frac{IH}{x_i^2+H^2} \ \ (i = 1,2,3,4) \tag{5}$$

Where K' is a constant magnification coefficient determined by the hardware circuit.

Two intermediate variables without specific physical meaning can be derived based on the magnitude of the direct voltage in (5).

$$A_1 = \frac{1}{U_1} - \frac{1}{U_2} = \frac{(x_1+x_2)(x_1-x_2)}{KK'IH} \tag{6}$$

$$A_2 = \frac{1}{U_3} - \frac{1}{U_4} = \frac{(x_3+x_4)(x_3-x_4)}{KK'IH} \tag{7}$$

Then (8) and (9) can be acquired based on the relative spatial layout of the four inductors.

$$x_1 - x_2 = x_3 - x_4 = -D \tag{8}$$

$$x_2 - x_3 = -L \tag{9}$$

From the (4) (5) (8) (9), $K, K', (x_1 - x_2), (x_3 - x_4)$ are all constants. *I* and *H* are determined by the general environment. $(x_1 + x_2)$ represents the distance from the navigation wire to the middle point of the inductors L_1 and L_2 , i.e. $((x_1 + x_2)/2, 0, H)$, along the X axis. So does $(x_3 + x_4)$. That is to say A_1 and A_2 can be utilized as the deviation from the signal wire to the sensors. However, A_1 and A_2 are also affected by the environment variables like *I* and *H*. Meanwhile, during the calculating process, repeated divide operation will decrease the precision of final result and lead to its vast fluctuation.

To overcome the disadvantages above and get the result with higher quality, this algorithm operates the above result as shown in (10).

$$\frac{A_2 + A_1}{A_2 - A_1} = \frac{U_1U_2U_4 - U_1U_2U_3 + U_2U_3U_4 - U_1U_3U_4}{U_1U_2U_4 - U_1U_2U_3 - U_2U_3U_4 + U_1U_3U_4} = \frac{(x_3 + x_4) + (x_1 + x_2)}{(x_3 + x_4) - (x_1 + x_2)} = \frac{2(x_1 + x_4)}{2D + 2L} \tag{10}$$

In (10), the term $2(x_1 + x_4)$ stands for the quadruple distance between the middle point $((x_1 + x_4)/2, H, 0)$ of the sensor row and the navigation wire. $2D + 2L$ is a constant related to the distribution of the sensors.

In the whole process of the four inputs $U_i(i = 1,2,3,4)$, only one divide operation is needed. According to this algorithm, the distance, marked as X, between the navigation wire and the middle point of the inductor row is amplified by four times, and the result is free from the influence of the current carrying by the navigation wire, the height of sensors themselves and other environmental factors.

In this system, X_1 and X_2 , as shown in Fig.6, which respectively represent the deviation of the front and back row, can be computed from the eight inductors in two rows. X_1 and X_2 are used for the control algorithm in the next section to implement the navigation.

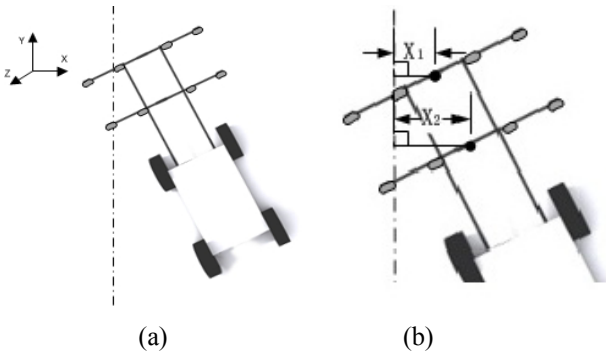

Fig. 6. X_1 and X_2

B. Generalization of the Path Calculation Algorithm

The proposed algorithm is based on the assumption that the navigation path is a long straight path. Its flexibility to adapt to various kinds of practical conditions such as the curved path and the crossing path (see Fig. 13) still need discussion.

For the curved path, the magnetic induction lines at the inner side are more intensive while the lines at the outside are sparser. Therefore, the inside induced voltage is larger whereas the outside is smaller compared to the condition of a straight path. The difference between both sides lead to the result that the calculated path position will deviate to the inner side compared to its real position. The robot will always run along the inner side of the curved path which will shorten the total running distance and improved the average speed. That is to say the running path of the robot is optimized naturally by this algorithm due to the magnetic field distribution.

The crossing path can be regarded as an overlying of two long vertical straight wires with different magnetic direction. As shown in Fig. 3, the inductors are only be able to directionally detect the magnetic field vertical to its central line but blind to the other one. Furthermore, the differential operation in the path calculation algorithm will also exclude the interference of it and ensure the accuracy of the detection.

V. CONTROL ALGORITHM

After figuring out the path, the steering servo and electric motor of the robot should be controlled to adjust its direction and speed to ensure the high-accuracy and high-speed tracing.

A. The Fuzzy PD Direction Controller

The direction of the robot should be adjusted in real time to trace the path. Any error of the steering servo control will lead to the deviation from the robot to the navigation path. At the same time, to trace at a high speed, the direction modification must response to the variations of the path rapidly and even has a good foresight of the path to compensate the lag caused by the computing and machinery factors. Hence, the direction control algorithm must be accurate and rapid.

Classic well-tuned PID control algorithm has the advantage of being simple, robust and accurate. However, it cannot adapt well to the various kinds of path conditions due to its constant parameters. Combining the strong adapting capability of fuzzy control and high accuracy of PID control algorithm, this system is able to modify the PD parameters K_p and K_d rapidly to optimize the control performance.

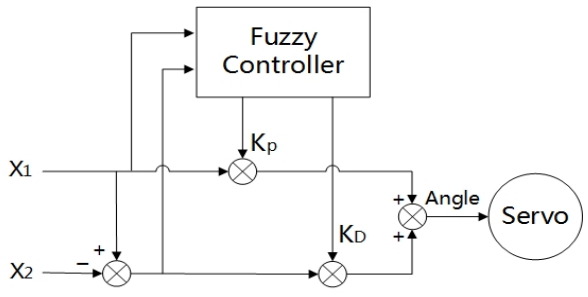

Fig. 7. The Fuzzy PD Direction Controller

Specifically, the control inputs of this system are X_1 and $X_1 - X_2$ resulted from section IV. X_1, the distance from the navigation wire to the middle point of the front row, represents the shifting of the whole robot. $X_1 - X_2$, the difference of relative distance of the front and back row, stands for the angle between the central axis of the robot and the wire. This angle can be used to predict the variation trend of the robot shifting distance relative to the navigation wire to improve its response performance. The general workflow is listed below.

- Step1: Fuzzify the Inputs: Taking both the accuracy and complexity into consideration, the fuzzy sets of X_1 and $X_1 - X_2$ can be deduced as {PB(Positive Big), PS(Positive Small), ZO(Zero), NS(Negative Small), NB(Negative Big)} to describe their variation range.
- Step2: Calculate Membership: The fuzzy linguistic values and the corresponding memberships of X_1 and $X_1 - X_2$ can be obtained based on Fig. 8.

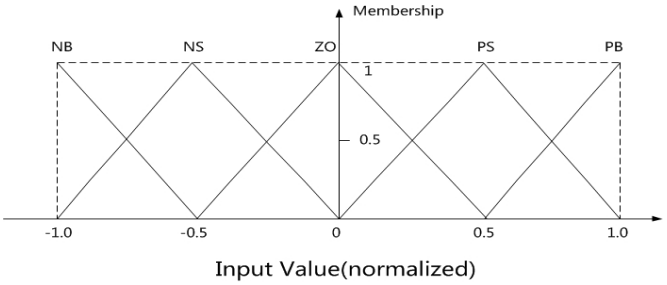

Fig. 8. The membership function of X_1 and $X_1 - X_2$

- Step 3: Establish the Fuzzy Rules Table: According to the practical drive experience, 25 strategies of computing normalized K_p and K_d are derived to establish the fuzzy control rules table as shown in table I and table II.

TABLE I. THE FUZZY RULES TABLE FOR K_P

K_p		X_1				
		NB	**NS**	**ZO**	**PS**	**PB**
$X_1 - X_2$	**NB**	1.0	0.5	0.2	0.2	0.2
	NS	0.6	0.3	0.2	0.2	0.2
	ZO	0.4	0.2	0.1	0.2	0.4
	PS	0.2	0.2	0.2	0.3	0.6
	PB	0.2	0.2	0.2	0.5	1.0

TABLE II. THE FUZZY RULES TABLE FOR K_D

K_d		X_1				
		NB	**NS**	**ZO**	**PS**	**PB**
$X_1 - X_2$	**NB**	1.0	0.8	0.7	0.8	0.8
	NS	0.8	0.7	0.5	0.7	0.8
	ZO	0.8	0.6	0.5	0.6	0.8
	PS	0.8	0.7	0.5	0.7	0.8
	PB	0.8	0.8	0.7	0.8	1.0

For example, small X_1 and $X_1 - X_2$ means the angle between the central axis of the robot and the navigation wire is small and without increasing tendency. That is to say, K_p should be small as well to finely turn the direction while K_d should be moderate to ensure the response. When X_1 is small

but $X_1 - X_2$ is large, K_d should be increased to adjust the direction quickly to adapt to the increasing trend of the shifting distance.

- Step 4: Fuzzy Reasoning and Defuzzify: the final output K_p can be calculated by centroid method, as (11). So is K_d calculated.

$$K_p = \sum_{i,j=1}^{i,j=5} R_{ij}\, m_{ij} n_{ij} \qquad (11)$$

Where m_{ij}, n_{ij} are the memberships of X_1 and $X_1 - X_2$ of the corresponding linguistic value, R_{ij} is the K_p value based on the rules table. ij means row i and column j of the table.

- Step 5: Calculate PD Output: Based on the K_p and K_d calculated above, the output of PD algorithm can be derived as (12) to get the steering servo control value.

$$\text{Angle} = K_p X_1 + K_d (X_1 - X_2) \qquad (12)$$

B. The Fuzzy Speed Controller

During the tracing, the robot should adjust its speed according to the navigating path in real time. Under the premise of following the path, the robot should go through different kinds of path as fast as possible.

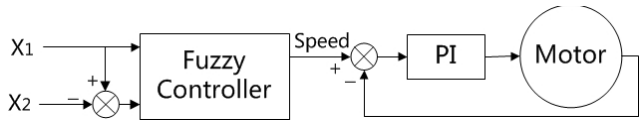

Fig. 9. The Fuzzy Speed Controller

Based on the navigation path, the controller calculates the real-time reference speed using the fuzzy control algorithm and controls the speed using a PI controller by close-loop control. The structure of the motor control algorithm is shown in Fig. 9.

The first two steps of the algorithm are the same as the direction control algorithm above.

Step 3: Establish the Fuzzy Rules Table: When X_1 and $X_1 - X_2$ are all very small, the robot should be running on a straight path. The speed should be increased and kept at a high level. When X_1 is small and $X_1 - X_2$ becomes static, the robot should be running in some curved path soon which means the speed should be decreased to turn the direction in time and get rid of side slipping out of the certain path caused by lacking of friction. If X_1 keeps still but $X_1 - X_2$ is small, the robot should be running in the middle of curved path where moderate speed is needed to keep the stable movement. Moreover, when their symbols are different, for example, X_1 is positive and $X_1 - X_2$ is negative, the robot may have shifting but close to the path which means the speed should be increased to go out of the curve. On the contrary, speed should be decreased.

According to the analysis as above, 25 rules of computing the normalized speed value are derived to establish the fuzzy control rules table as shown in table III.

TABLE III. THE FUZZY RULES TABLE FOR SPEED

Speed		X_1				
		NB	**NS**	**ZO**	**PS**	**PB**
$X_1 - X_2$	**NB**	0.5	0.6	1.0	1.0	1.0
	NS	0.5	0.6	1.0	1.0	0.9
	ZO	0.8	0.9	1.0	0.9	0.8
	PS	0.9	1.0	1.0	0.6	0.5
	PB	1.0	1.0	1.0	0.6	0.5

Step 4: Fuzzy Reasoning and Defuzzify:

$$\text{Speed} = \sum_{i,j=1}^{i,j=5} R_{ij}\, m_{ij} n_{ij} \qquad (13)$$

The output is regarded as the reference speed and input to the speed closed loop. With proper parameters for the PI controller, the robot are able to achieve the optimal speed control performance.

VI. EXPERIMENTS AND RESULTS

A. Path Detection Experiment

By manually moving the robot along the horizontal axis X, the sensors in the front row are used to verify the accuracy of the path calculation algorithm. The deviation values are recorded every 10mm when it varied from -100mm to 100mm. More results shown in Fig.10 can be obtained by repeating the experiment with different signal current, sensor height and the angle θ between the central axis of the robot and the navigation wire.

In Fig.10, Curve 1 represents the result which is close to the real deviation when the sensor height is 8cm and the current is 100mA. Within the range of -50mm ~ 50mm, the error is less than ± 3mm while ± 5mm when the range changed to -100mm ~ 100mm. Comparing Curve 2 and 3 which are both calculated at the height of 8cm with respectively 50mA and 150mA wire current, the error is still within ± 5mm. That is to say, the variety of current has rarely influence on the precision of final results with this algorithm. Curve 4 shows the descending of precision deduced from the results with 12 cm in height and 100mA current. The error is 17mm at the point of 100mm due to the reason of dropping magnetic intensity opposite to the increasing height. Meanwhile, according to formula (3), as H increases, the induced voltage will be easily interfered by the surroundings which may lead to the decreasing accuracy. Curve 5 shows the influence of the angle θ. The precision dropped down a little when θ is 30 degree.

In practical condition, the deviation between the robot and the navigation wire are kept in a small range in order to trace the path. The absolute error of detecting in this system stays within 5mm when the deviation of robot vary within -50mm to 50mm under different current and height conditions, which satisfies the requirement of high-accuracy and high-speed navigation.

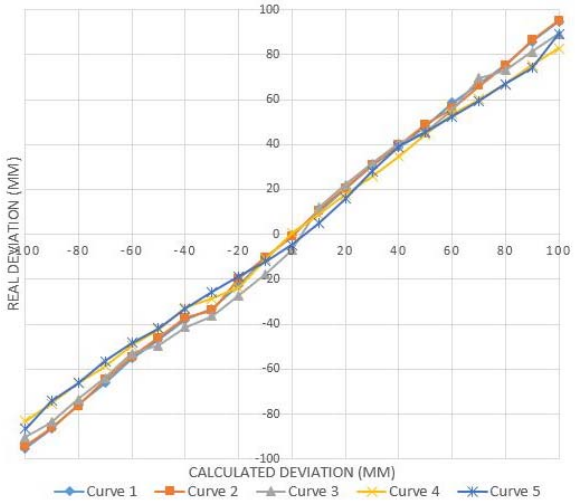

Fig. 10. Calculated deviation under different conditions

B. Magnetic Navigation Experiment

To verify the effectiveness of the control algorithm, three parameters are chosen to record the condition of the robot during its automatically running on the path shown in Fig.11. The data are shown in Fig.12.

Fig. 11. Test Path A

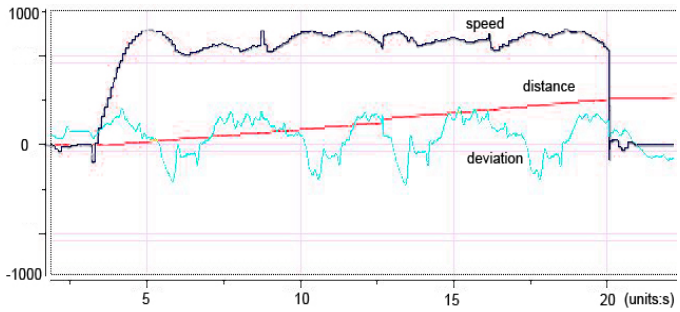

Fig. 12. Real-time navigation control data

In Fig.12, the green curve presents X_1(normalized to 1000), which is the horizontal deviation from the middle point of the front row to the navigation wire, changes over time. The value of X_1 fluctuated around zero. Every big change represents once direction turning while the small waves overlying on it stand for continuously modification of the direction during the processing of tracing the path. The short zero line between big changing is the result of short straight path. Comparing Fig. 11 and 12, the green curve corresponds preciously and quickly to the turning in real trace. The varying range of X_1 is only one third of the maximum value, which illustrates the excellent tracing accuracy of the magnetic navigation. The blue curve is the changing of running speed (normalized to 1000) over time. The robot kept running in a middle-high speed of 2.3m/s. The overall performance shows the characters of decelerating when entering the curve, accelerating when exiting and preserving high speed on straight path. The red curve is total running distance (normalized to 1000).

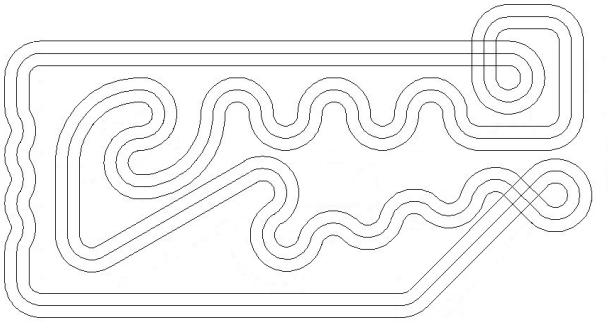

Fig. 13. Test Path B

Another test path is shown in Fig. 13, of which the ratio of straight path and curved path is about 1.0 and the total length is 70.3m. The speed of the robot varies from 1.9 to 3.4 m/s, and the overall average speed is 2.9 m/s. Taking the scale of the robot itself (0.45m) into consideration, this is a relatively high automatic navigation speed. The speed limit factors at this time are mainly the wheel ground adhesion, drive capability and the mechanical characters of the robot.

VII. CONCLUSION

This paper proposes an accurate navigation path detection algorithm which calculates the position of the path relative to the robot, and free from the influence of the environment conditions. Meanwhile, the fuzzy control and PID algorithm are combined to optimize the control performance of the steering servo and the electrical motor. A wheeled mobile robot is built to verify the detection and control algorithm. The results show that the wheeled mobile robot can trace the navigation path automatically and precisely at a high speed. The results of this system encourage further investigations of magnetic navigation in different application fields.

REFERENCES

[1] Carpi, Federrico, and C. Pappone, “Magnetic maneuvering of endoscopic capsules by means of a robotic navigation system,” . IEEE Trans on. Biomedical Engineering. vol. 56, pp. 1482-1490, May 2009.

[2] T. H Riehle, S.M.Anderson, P.A. Lichter, N.A.Giudice, and D.S,. "Indoor magnetic navigation for the blind," IEEE Engineering in Medicine and Biology Society (EMBC), CA, pp.1972-1975, Sep. 2012.

[3] Y. Bai, L. Yang, and C. Dong. "Electromagnetic Navigation Smart Car Control System Based on MC9S128," Measurement & Control Technology, vol.021, Jan. 2011.

[4] Y. Liu, W. Zhang, X. Liu, and S. Qiu. "Study on electromagnetic navigation intelligent vehicle detection and control system,"Transducer and Microsystem Technologies, vol. 021, Apr. 2012.

[5] H. Wang, and Y. Hu, "Design and Realization of the Smart Magnetic Navigation Car System." Process Automation Instrumentation, vol. 003, pp.5-8, Nov.2011.